

Domain Adaptation for Time Series Forecasting via Attention Sharing

Xiaoyong Jin ^{*} Youngsuk Park [†] Danielle C. Maddix [†] Hao Wang [†]
Yuyang Wang [†]

Abstract

Recently, deep neural networks have gained increasing popularity in the field of time series forecasting. A primary reason for their success is their ability to effectively capture complex temporal dynamics across multiple related time series. The advantages of these deep forecasters only start to emerge in the presence of a sufficient amount of data. This poses a challenge for typical forecasting problems in practice, where there is a limited number of time series or observations per time series, or both. To cope with this data scarcity issue, we propose a novel domain adaptation framework, Domain Adaptation Forecaster (DAF). DAF leverages statistical strengths from a relevant domain with abundant data samples (source) to improve the performance on the domain of interest with limited data (target). In particular, we use an attention-based shared module with a domain discriminator across domains and private modules for individual domains. We induce domain-invariant latent features (queries and keys) and retrain domain-specific features (values) simultaneously to enable joint training of forecasters on source and target domains. A main insight is that our design of aligning keys allows the target domain to leverage source time series even with different characteristics. Extensive experiments on various domains demonstrate that our proposed method outperforms state-of-the-art baselines on synthetic and real-world datasets, and ablation studies verify the effectiveness of our design choices.

1 Introduction

Similar to other fields with predictive tasks, time series forecasting has recently benefited from the development of deep neural networks [Flunkert et al., 2020, Borovykh et al., 2017, Oreshkin et al., 2020a, Park et al., 2021]. In particular, based on the success of Transformer models in natural language processing [Vaswani et al., 2017], attention models have also been effectively applied to forecasting [Li et al., 2019, Lim et al., 2019]. While these deep forecasting models excel at capturing complex temporal dynamics from a sufficiently large time series dataset, it is often challenging in practice to collect enough data.

A common solution to the data scarcity problem is to introduce another dataset with abundant data samples from a so-called source domain related to the dataset of interest, referred to as the target domain. For example, traffic data from an area with an abundant number of sensors (source domain) can be used to train a model to forecast the traffic flow in an area with insufficient monitoring recordings (target domain). However, deep neural networks trained on one domain can be poor at generalizing to another domain due to the issue of domain shift, that is, the distributional discrepancy between domains [Wang et al., 2021].

Domain adaptation (DA) methods attempt to mitigate the harmful effect of domain shift by aligning features extracted across source and target domains [Ganin et al., 2016, Bousmalis et al., 2016, Hoffman et al., 2018, Bartunov and Vetrov, 2018]. Existing approaches mainly focus on classification tasks, where a classifier learns a mapping from a learned domain-invariant latent space to a fixed label space using source data. Consequently, the classifier depends only on common features across domains, and can be applied to the target domain [Wilson and Cook, 2020].

There are two main challenges in directly applying existing DA methods to time series forecasting. First, due to the temporal nature of time series, evolving patterns within time series are not likely to be captured by

^{*}University of California, Santa Barbara. Work conducted during internship at Amazon

[†]AWS AI Lab

Correspondence to Xiaoyong Jin <x_jin@cs.ucsb.edu>, Youngsuk Park <pyoungsu@amazon.com>

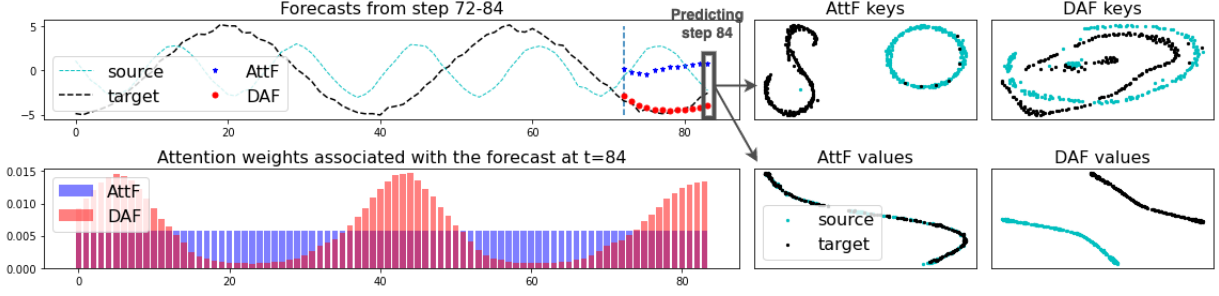


Figure 1: Forecasts of single-domain attention-based forecaster (AttF) and our cross-domain forecaster (DAF). Sample forecasts from steps 72-84 on traffic data where our DAF uses household electricity data as source data (*top left*). Bar plot of the weights on the context history of the attention distributions of AttF and DAF associated with forecasting step 84 (*bottom left*). Attention keys (*top right*) and values (*bottom right*) of AttF and DAF after dimension reduction to 2D. The keys and values of AttF in the source domain are generated by simply applying AttF model trained on target data to the source data. The strategy of aligning keys rather than values between source and target domains in our DAF captures the correct attention weights, as illustrated by the accurate forecasts compared to AttF (cf. red dots vs. blue dots from steps 72-84).

a representation of the entire history. Future predictions may depend on local patterns within different time periods, and a sequence of *local representations* can be more appropriate than using the *entire history* as done with most conventional approaches. Second, the *output space* in forecasting tasks is not fixed across domains in general since a forecaster generates a time series following the input, which is domain-dependent, e.g. kW in electrical source data vs. unit count in stock target data. Both domain-invariant and domain-specific features need to be extracted and incorporated in forecasting to model domain-dependent properties so that the data distribution of the respective domain is properly approximated. Hence, we need to carefully design the type of features to be shared or non-shared over different domains, and to choose a suitable architecture for our time-series forecasting model.

We propose to resolve the two challenges using an attention-based model Vaswani et al. [2017] equipped with domain adaptation. First, for evolving patterns, attention models can make dynamic forecasts based on a combination of values weighted by time-dependent query-key alignments. Second, as the alignments in an attention module are independent of specific patterns, the queries and keys can be induced to be domain-invariant while the values can stay domain-specific for the model to make domain-dependent forecasts. Figure 1 presents an illustrative example of a comparison between a conventional attention-based forecaster (AttF) and its counterpart combined with our domain adaptation strategy (DAF) on synthetic datasets with sinusoidal signals. While AttF is trained using limited target data, DAF is jointly trained on both domains. By aligning the keys across domains as the top rightmost panel shows, the context matching learned in the source domain helps DAF generate more reasonable attention weights that focus on the same phases in previous periods of target data than the uniform weights generated by AttF in the bottom left panel. The bottom right panels illustrate that the single-domain AttF produces the same values for both domains as the input is highly overlapped, while DAF is able to generate distinct values for each domain. As a result, the top left panel shows that DAF produces more accurate domain-specific forecasts than AttF does.

In this paper, we propose the Domain Adaptation Forecaster (DAF), a novel method that effectively solves the data scarcity issue in time series forecasting by applying domain adaptation techniques via attention sharing. The main contributions of this paper are:

1. In DAF, we propose a new architecture that properly induces and combines domain-invariant and domain-specific features to make multi-horizon forecasts for source and target domains through a shared attention module. To the best of our knowledge, our work provides the first end-to-end DA solution specific for multi-horizon forecasting tasks with adversarial training.
2. We demonstrate that DAF outperforms state-of-the-art single-domain forecasting and domain adaptation baselines in terms of accuracy in a data-scarce target domain through extensive synthetic and real-world experiments that solve cold-start and few-shot forecasting problems.
3. We perform extensive ablation studies to show the importance of the domain-invariant features induced

by a discriminator and the retrained domain-specific features in our DAF model, and that our designed sharing strategies with the discriminator result in better performance than other potential variants.

2 Related Work

Deep neural networks have been introduced to time series forecasting with considerable successes [Flunkert et al., 2020, Borovykh et al., 2017, Oreshkin et al., 2020a, Wen et al., 2017, Wang et al., 2019, Sen et al., 2019, Rangapuram et al., 2018]. In particular, attention-based transformer-like models [Vaswani et al., 2017] have achieved state-of-the-art performance [Li et al., 2019, Lim et al., 2019, Wu et al., 2020, Zhou et al., 2021]. A downside to these sophisticated models is their reliance on a large dataset with homogeneous time series to train. Once trained, the deep learning models may not generalize well to a new domain of exogenous data due to domain shift issues [Wang et al., 2005, Purushotham et al., 2017, Wang et al., 2021].

To solve the domain shift issue, domain adaptation has been proposed to transfer knowledge captured from a source domain with sufficient data to the target domain with unlabeled or insufficiently labeled data for various tasks [Motiian et al., 2017, Wilson and Cook, 2020, Ramponi and Plank, 2020]. In particular, sequence modeling tasks in natural language processing mainly adopt a paradigm where large transformers are successively pre-trained on a general domain and fine-tuned on the task domain [Devlin et al., 2019, Han and Eisenstein, 2019, Gururangan et al., 2020, Rietzler et al., 2020]. It is not immediate to directly apply these methods to forecasting scenarios due to several challenges. First, it is difficult to find a common source dataset in time series forecasting to pre-train a large forecasting model. Second, it is expensive to pre-train a different model for each target domain. Third, the predicted values are not subject to a fixed vocabulary, heavily relying on extrapolation. Lastly, there are many domain-specific confounding factors that cannot be encoded by a pre-trained model.

An alternative approach to pre-training and fine-tuning for domain adaptation is to extract domain-invariant representations from raw data [Ben-David et al., 2010, Cortes and Mohri, 2011]. Then a recognition model that learns to predict labels using the source data can be applied to the target data. In their seminal works, Ganin and Lempitsky [2015], Ganin et al. [2016] propose DANN to obtain domain invariance by confusing a domain discriminator that is trained to distinguish representations from different domains. A series of works follow this adversarial training paradigm [Tzeng et al., 2017, Zhao et al., 2018, Alam et al., 2018, Wright and Augenstein, 2020], and outperform conventional metric-based approaches [Long et al., 2015, Chen et al., 2020, Guo et al., 2020] in various applications of domain adaptation. However, these works do not consider the task of time series forecasting, and address the challenges in the introduction accordingly.

In light of successes in related fields, domain adaptation techniques have been introduced to time series tasks [Purushotham et al., 2017, Wilson et al., 2020]. Cai et al. [2021] aim to solve domain shift issues in classification and regression tasks by minimizing the discrepancy of the associative structure of time series variables between domains. A limitation of this metric-based approach is that it cannot handle the multi-horizon forecasting task since the label is associated with the input rather than being pre-defined. Hu et al. [2020] propose DATSING to adopt adversarial training to fine-tune a pre-trained forecasting model by augmenting the target dataset with selected source data based on pre-defined metrics. This approach lacks the efficiency of end-to-end solutions due to its two-stage nature. In addition, it does not consider domain-specific features to make domain-dependent forecasts. Lastly, Ghifary et al. [2016], Bousmalis et al. [2016], Shi et al. [2018] make use of domain-invariant and domain-specific representations in adaptation. However, since these methods do not accommodate the sequential nature of time series, they cannot be directly applied to forecasting.

3 Domain Adaptation in Forecasting

Time Series Forecasting Suppose a set of N time series, and each consists of observations $z_{i,t} \in \mathbb{R}$, associated with optional input covariates $\xi_{i,t} \in \mathbb{R}^d$ such as price and promotion, at time t . In time series forecasting, given T past observations and all future input covariates, we wish to make τ multi-horizon future predictions at time T via model F :

$$z_{i,T+1}, \dots, z_{i,T+\tau} = F(z_{i,1}, \dots, z_{i,T}; \xi_{i,1}, \dots, \xi_{i,T+\tau}). \quad (1)$$

In this paper, we focus on the scenario where little data is available for the problem of interest while sufficient data from other sources is provided. For example, one or both of the number of time series N and the length T is limited. For notation simplicity, we drop the covariates $\{\xi_{i,t}\}_{t=1}^{T+\tau}$ in the following. We denote the dataset $\mathcal{D} = \{(\mathbf{X}_i, \mathbf{Y}_i)\}_{i=1}^N$ with past observations $\mathbf{X}_i = [z_{i,t}]_{t=1}^T$ and future ground truths $\mathbf{Y}_i = [z_{i,t}]_{t=T+1}^{T+\tau}$ for the i -th time series. We also omit the index i when the context is clear.

Adversarial Domain Adaptation in Forecasting To find a suitable forecasting model F in equation (1) on a data-scarce time series dataset, we cast the problem in terms of a domain adaptation problem, given that another “relevant” dataset is accessible. In the domain adaption setting, we have two types of data: source data \mathcal{D}_S with abundant samples and target data \mathcal{D}_T with limited samples. Our goal is to produce an accurate forecast on the target domain \mathcal{T} , where little data is available, by leveraging the data in the source domain \mathcal{S} . Since our goal is to provide a forecast in the target domain, in the remainder of the text, we use T and τ to denote the target historical length and target prediction length, respectively, and also use the subscript \mathcal{S} for the corresponding quantities in the source data \mathcal{D}_S , and likewise for \mathcal{T} .

To compute the desired target prediction $\hat{\mathbf{Y}}_i = [\hat{z}_{i,t}]_{t=T+1}^{T+\tau}$, $i = 1, \dots, N$, we optimize the training error on both domains jointly and in an adversarial manner in the following minimax problem:

$$\min_{G_S, G_T} \max_D \mathcal{L}_{seq}(\mathcal{D}_S; G_S) + \mathcal{L}_{seq}(\mathcal{D}_T; G_T) - \lambda \mathcal{L}_{dom}(\mathcal{D}_S, \mathcal{D}_T; D, G_S, G_T), \quad (2)$$

where the parameter $\lambda \geq 0$ balances between the estimation error \mathcal{L}_{seq} and the domain classification error \mathcal{L}_{dom} . Here, G_S, G_T denote sequence generators that estimate sequences in each domain, respectively, and D denotes a discriminator that classifies the domain between source and target.

We first define the estimation error \mathcal{L}_{seq} induced by a sequence generator G as follows:

$$\mathcal{L}_{seq}(\mathcal{D}; G) = \sum_{i=1}^N \left(\frac{1}{T} \sum_{t=1}^T l(z_{i,t}, \hat{z}_{i,t}) + \frac{1}{\tau} \sum_{t=T+1}^{T+\tau} l(z_{i,t}, \hat{z}_{i,t}) \right), \quad (3)$$

where l is a loss function and estimation $\hat{z}_{i,t}$ is the output of a generator G , and each term in equation (3) represents the error of input reconstruction and future prediction, respectively. Next, let $\mathcal{H} = \{h_{i,t}\}_{i=1, t=1}^{N, T+\tau}$ be a set of some latent feature $h_{i,t}$ induced by generator G . Then, the domain classification error \mathcal{L}_{dom} in equation (2) denotes the cross-entropy loss in the latent spaces as follows:

$$\begin{aligned} \mathcal{L}_{dom}(\mathcal{D}_S, \mathcal{D}_T; D, G_S, G_T) = & -\frac{1}{|\mathcal{H}_S|} \sum_{h_{i,t} \in \mathcal{H}_S} \log D(h_{i,t}) \\ & -\frac{1}{|\mathcal{H}_T|} \sum_{h_{i,t} \in \mathcal{H}_T} \log [1 - D(h_{i,t})], \end{aligned} \quad (4)$$

where \mathcal{H}_S and \mathcal{H}_T are latent feature sets associated with the source \mathcal{D}_S and target \mathcal{D}_T , and $|\mathcal{H}|$ denotes the cardinality of a set \mathcal{H} . The minimax objective equation (2) is optimized via adversarial training alternately. In the following subsections, we propose specific design choices for G_S, G_T (see subsection 4.1) and the latent features $\mathcal{H}_S, \mathcal{H}_T$ (see subsection 4.2) in our DAF model.

4 The Domain Adaptation Forecaster (DAF)

We propose a novel strategy based on attention mechanism to perform domain adaptation in forecasting. The proposed solution, the Domain Adaptation Forecaster (DAF), employs a sequence generator to process time series from each domain. Each sequence generator consists of an encoder, an attention module and a decoder. As each domain provides data with distinct patterns from different spaces, we keep the encoders and decoders privately owned by the respective domain. The core attention module is shared by both domains for

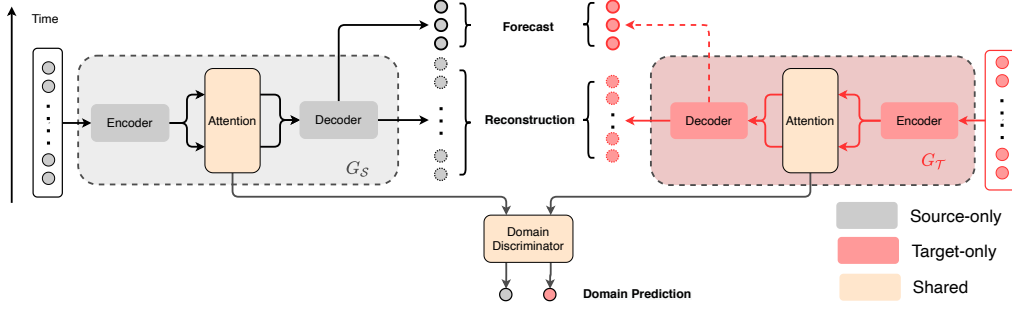


Figure 2: An architectural overview of DAF. The grey modules belong to the source domain, and red modules belong to target domain. The attention modules and domain discriminators shown in beige are shared by both domains. The model takes the historical portion of a time series as input, and produces a reconstruction of input and a forecast of the future time steps. The domain discriminator is a binary classifier, and predicts the origin of an intermediate representation within the attention module, either the source or the target.

adaptation. In addition to computing future predictions, the generator also reconstructs the input to further guarantee the effectiveness of the learned representations. Figure 2 illustrates an overview of the proposed architecture.

4.1 Sequence Generators

In this subsection, we discuss our design of the sequence generators G_S, G_T in equation (2). Since the generators for both domains have the same architecture, we omit the domain index of all quantities and denote either generator by G in the following paragraphs by default. The generator G in each domain processes an input time series $\mathbf{X} = [z_t]_{t=1}^T$ and generates the reconstructed sequence $\hat{\mathbf{X}}$ and the predicted future $\hat{\mathbf{Y}}$.

Private Encoders The private encoder transforms the raw input \mathbf{X} into the pattern embedding $\mathbf{P} = [\mathbf{p}_t]_{t=1}^T$ and value embedding $\mathbf{V} = [\mathbf{v}_t]_{t=1}^T$. For the value embedding, we apply a position-wise MLP with parameter θ_v to encode input $\mathbf{X} = [z_t]_{t=1}^T$

$$\mathbf{v}_t = \text{MLP}(z_t; \theta_v).$$

For the pattern embedding \mathbf{P} , we apply M independent temporal convolutions with various kernel sizes in order to extract short-term patterns at different scales. Specifically, for $j = 1, \dots, M$, each convolution with parameter θ_p takes the input \mathbf{X} to give a sequence of local representations,

$$\mathbf{p}^j = \text{Conv}(\mathbf{X}; \theta_p^j).$$

We concatenate each \mathbf{p}_t^j to build a multi-scale pattern embedding $\mathbf{p}_t = [\mathbf{p}_t^j]_{j=1}^M$ and $\mathbf{P} = [\mathbf{p}_t]_{t=1}^T$ with parameters $\theta_p = [\theta_p^j]_{j=1}^M$ accordingly. To avoid dimension issues from the concatenation, we keep the dimension of \mathbf{P} and \mathbf{V} the same. The extracted pattern \mathbf{P} and value \mathbf{V} are fed into the shared attention module.

Shared Attention Module We design the attention module to be shared by both domains since its primary task is to generate domain-invariant queries \mathbf{Q} and keys \mathbf{K} from pattern embeddings \mathbf{P} for both source and target domains. Formally, we project \mathbf{P} into d -dimensional queries $\mathbf{Q} = [\mathbf{q}_t]_{t=1}^T$ and keys $\mathbf{K} = [\mathbf{k}_t]_{t=1}^T$ via a position-wise MLP

$$(\mathbf{q}_t, \mathbf{k}_t) = \text{MLP}(\mathbf{p}_t; \theta_s).$$

As a result, the patterns from both domains are projected into a common space, which is later induced to be domain-invariant via adversarial training. At time t , an attention score α is computed as the normalized

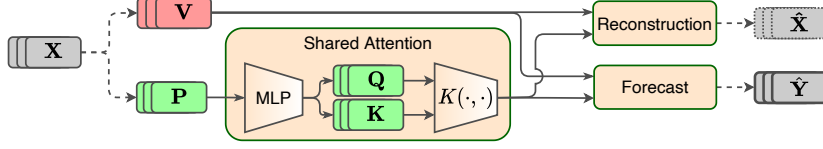


Figure 3: In DAF, the shared attention module processes pattern and value embeddings from either domain. A kernel function encodes pattern embeddings to a shared latent space for weight computation. We combine value embeddings by different groups of weights to obtain the interpolation $t \leq T$ for reconstruction $\hat{\mathbf{X}}$ and the extrapolation $t = T + 1$ for the forecast $\hat{\mathbf{Y}}$.

alignment between the query \mathbf{q}_t and keys $\mathbf{k}_{t'}$ at neighborhood positions $t' \in \mathcal{N}(t)$ using a positive semi-definite kernel $\mathcal{K}(\cdot, \cdot)$,

$$\alpha(\mathbf{q}_t, \mathbf{k}_{t'}) = \frac{\mathcal{K}(\mathbf{q}_t, \mathbf{k}_{t'})}{\sum_{t' \in \mathcal{N}(t)} \mathcal{K}(\mathbf{q}_t, \mathbf{k}_{t'})}, \quad (5)$$

e.g. an exponential scaled dot-product $\mathcal{K}(\mathbf{q}, \mathbf{k}) = \exp\left(\frac{\mathbf{q}^T \mathbf{k}}{\sqrt{d}}\right)$. Then, a representation \mathbf{o}_t is produced as the average of values $\mathbf{v}_{\mu(t')}$ weighted by attention score $\alpha(\mathbf{q}_t, \mathbf{k}_{t'})$ on neighborhood $\mathcal{N}(t)$, followed by a MLP with parameter θ_o :

$$\mathbf{o}_t = \text{MLP} \left(\sum_{t' \in \mathcal{N}(t)} \alpha(\mathbf{q}_t, \mathbf{k}_{t'}) \mathbf{v}_{\mu(t')} ; \theta_o \right), \quad (6)$$

where $\mu : \mathbb{N} \rightarrow \mathbb{N}$ is a position translation. The choice of $\mathcal{N}(t)$ and $\mu(t)$ depends on whether G is in interpolation mode for reconstruction when $t \leq T$ or extrapolation mode for forecasting when $t > T$. See appendix A for details on $\mathcal{N}(t)$ and $\mu(t)$ selections.

Private Decoders The private decoder produces prediction \hat{z}_t out of \mathbf{o}_t through another position-wise MLP: $\hat{z}_t = \text{MLP}(\mathbf{o}_t; \theta_d)$. By doing so, we can generate reconstructions $\hat{\mathbf{X}} = [\hat{z}_t]_{t=1}^T$ and the one-step prediction \hat{z}_{T+1} . This prediction \hat{z}_{T+1} is fed back into the encoder and attention model to predict the next one-step ahead prediction. We recursively feed the prior predictions to generate the predictions $\hat{\mathbf{Y}} = [\hat{z}_t]_{t=T+1}^{T+\tau}$ over τ time steps.

4.2 Domain Discriminator

In order to induce the queries and keys of the attention module to be domain-invariant, a domain discriminator is introduced to classify the origin of a given query or key. We employ a position-wise MLP $D : \mathbb{R}^d \rightarrow [0, 1]$:

$$D(\mathbf{q}_t) = \text{MLP}(\mathbf{q}_t; \theta_D), \quad D(\mathbf{k}_t) = \text{MLP}(\mathbf{k}_t; \theta_D).$$

The discriminator D performs binary classifications on whether \mathbf{q}_t and \mathbf{k}_t originate from the source or target domain by minimizing the cross entropy loss of \mathcal{L}_{dom} in equation (4). We design the latent features $\mathcal{H}_S, \mathcal{H}_T$ in equation (4) to be the keys $\mathbf{K} = [\mathbf{k}_t]_{t=1}^{T+\tau}$ and queries $\mathbf{Q} = [\mathbf{q}_t]_{t=1}^{T+\tau}$ in both source and target domains, respectively.

4.3 Adversarial Training

Recall we have defined generators G_S, G_T based on the private encoder/decoder and the shared attention module. The discriminator D induces the invariance of latent features keys \mathbf{K} and queries \mathbf{Q} across domains. While D tries to classify the domain between source and target, G_S, G_T are trained to confuse D . By choosing the MSE loss for l , the minimax objective in equation (2) is now formally defined over generators G_S, G_T with parameters $\Theta_G = \{\theta_p^S, \theta_v^S, \theta_d^S, \theta_p^T, \theta_v^T, \theta_d^T, \theta_s, \theta_o\}$ and domain discriminator D with parameter θ_D . Algorithm 1 summarizes the training routine of DAF. We alternately update Θ_G and θ_D in opposite directions so that $G = \{G_S, G_T\}$ and D are trained adversarially. Here, we use a standard pre-processing for \mathbf{X}, \mathbf{Y} and post-processing for $\hat{\mathbf{X}}, \hat{\mathbf{Y}}$.

Algorithm 1 Adversarial Training of DAF

```
1: Input: dataset  $\mathcal{D}_S, \mathcal{D}_T$ ; epochs  $E$ , step sizes  
2: Initialization: parameter  $\Theta_G$  for generator  $G_S, G_T$ , parameter  $\theta_D$  for discriminator  $D$   
3: for epoch = 1 to  $E$  do  
4:   repeat  
5:     sample  $\mathbf{X}_S, \mathbf{Y}_S \sim \mathcal{D}_S$  and  $\mathbf{X}_T, \mathbf{Y}_T \sim \mathcal{D}_T$   
6:     generate  $\hat{\mathbf{X}}_S, \hat{\mathbf{Y}}_S = G_S(\mathbf{X}_S)$  and  $\hat{\mathbf{X}}_T, \hat{\mathbf{Y}}_T = G_T(\mathbf{X}_T)$   
7:     compute  $\mathcal{L}_{seq}$  in equation (3) for  $S$  and  $T$ ,  $\mathcal{L}_{dom}$  in equation (4), and total  $\mathcal{L}$  in equation (2)  
8:     gradient descent with  $\nabla_{\Theta_G} \mathcal{L}$  to update  $G_S, G_T$   
9:     gradient ascent with  $\nabla_{\theta_D} \mathcal{L}$  to update  $D$   
10:   until  $\mathcal{D}_T$  is exhausted  
11: end for
```

5 Experiments

We conduct extensive experiments to demonstrate the effectiveness of the proposed DAF in adapting from a source domain to a target domain, leading to accuracy improvement over state-of-the-art forecasters and existing DA ethos. In addition, we conduct ablation studies to examine the contribution of our design to the significant performance improvement.

5.1 Baselines and Evaluation

In the experiments, we compare DAF with the following single-domain and cross-domain baselines. The conventional single-domain forecasters trained only on the target domain include:

- DAR: DeepAR [Flunkert et al., 2020];
- VT: Vanilla Transformer [Vaswani et al., 2017];
- AttF: the sequence generator G_T for the target domain trained by minimizing $\mathcal{L}_{seq}(\mathcal{D}_T; G_T)$ in equation (2).

The cross-domain forecasters trained on both source and target domain include:

- DATSING: pretrained and finetuned forecaster Hu et al. [2020];
- RDA: RNN-based DA forecaster obtained by replacing the attention module in DAF with a LSTM module and inducing the domain-invariance of LSTM encodings. Specifically, we consider three variants:
 - RDA-DANN: adversarial DA via gradient reversing Ganin et al. [2016];
 - RDA-ADDA: adversarial DA via GAN-like optimization Tzeng et al. [2017];
 - RDA-MMD: metric based DA via minimizing MMD between LSTM encodings Li et al. [2017].

We implement the models using PyTorch [Paszke et al., 2019], and train them on AWS Sagemaker [Liberty et al., 2020]. For DAR, we call the publicly available version on Sagemaker. In most of the experiments, DAF and the baselines are tuned on a held-out validation set. See appendix C.2 for details on the model configurations and hyperparameter selections.

We evaluate the forecasting error in terms of the Normalized Deviation (ND) [Yu et al., 2016]:

$$\text{ND} = \left(\sum_{i=1}^N \sum_{t=T+1}^{T+\tau} |z_{i,t} - \hat{z}_{i,t}| \right) / \left(\sum_{i=1}^N \sum_{t=T+1}^{T+\tau} |z_{i,t}| \right),$$

where $\mathbf{Y}_i = [z_{i,t}]_{t=T+1}^{T+\tau}$ and $\hat{\mathbf{Y}}_i = [\hat{z}_{i,t}]_{t=T+1}^{T+\tau}$ denote the ground truths and predictions, respectively. In the subsequent tables, the methods with a mean ND metric within one standard deviation of method with the lowest mean ND metric are shown in bold.

5.2 Synthetic Datasets

We first simulate scenarios suited for domain adaptation, namely **cold-start** and **few-shot** forecasting. In both scenarios, we consider a source dataset \mathcal{D}_S and a target dataset \mathcal{D}_T consisting of time-indexed sinusoidal signals with random parameters, including amplitude, frequency and phases, sampled from different uniform

| Task | N | T | τ | DAR | VT | AttF | DATSING | RDA-ADDA | DAF |
|------------|------|-----|--------|--------------------|-------------|-------------|-------------|--------------------|--------------------|
| Cold Start | 5000 | 36 | 18 | 0.053±0.003 | 0.040±0.001 | 0.042±0.001 | 0.039±0.004 | 0.035±0.002 | 0.035±0.003 |
| | | 45 | | 0.037±0.002 | 0.039±0.001 | 0.041±0.004 | 0.039±0.002 | 0.034±0.001 | 0.030±0.003 |
| | | 54 | | 0.031±0.002 | 0.039±0.001 | 0.038±0.005 | 0.037±0.001 | 0.034±0.001 | 0.029±0.003 |
| Few Shot | 20 | 144 | | 0.062±0.003 | 0.089±0.001 | 0.095±0.003 | 0.078±0.005 | 0.059±0.003 | 0.057±0.004 |
| | 50 | | | 0.059±0.004 | 0.085±0.001 | 0.074±0.005 | 0.076±0.006 | 0.054±0.003 | 0.055±0.001 |
| | 100 | | | 0.059±0.003 | 0.079±0.002 | 0.071±0.002 | 0.058±0.005 | 0.053±0.007 | 0.051±0.001 |

Table 1: Performance comparison of DAF on synthetic datasets with varying historical lengths T (cold-start), and varying number of time series N (few-shot) and prediction length τ in terms of the mean \pm the standard deviation ND metric. The winners and the competitive followers (the gap is smaller than its standard deviation over 5 runs) are bolded for reference.

distributions. See appendix B for details on the data generation. The total observations in the target dataset are limited in both scenarios by either length or number of time series.

Cold-start forecasting aims to forecast in a target domain, where the signals are fairly short and limited historical information is available for future predictions. To simulate solving the cold-start problem, we set the time series historical length in the source data $T_S = 144$, and vary the historical length in the target data T within $\{36, 45, 54\}$. The period of sinusoids in the target domain is fixed to be 36, so that the historical observations cover $1 \sim 1.5$ periods. We also fix the number of time series $N_S = N = 5000$.

Few-shot forecasting occurs when there is an insufficient number of time series in the target domain for a well-trained forecaster. To simulate this problem, we set the number of time series in the source data $N_S = 5000$, and vary the number of time series in the target data N within $\{20, 50, 100\}$. We also fix the historical lengths $T_S = T = 144$. The prediction length is set to be equal for both source and target datasets, i.e. $\tau_S = \tau = 18$.

The results of the synthetic experiments on the cold-start and few-shot problems in Table 1 demonstrate that the performance of DAF is better than or on par with the baselines in all experiments. We also note the following observations to provide a better understanding into domain adaptation methods. First, we see that the cross-domain forecasters RDA and DAF that are jointly trained end-to-end using both source and target data are overall more accurate than the single-domain forecasters. This finding indicates that source data is helpful in forecasting the target data. Second, among the cross-domain forecasters DATSING is outperformed by RDA and DAF, indicating the importance of joint training on both domains. Third, on a majority of the experiments our attention-based DAF model is more accurate than or competitive to the RNN-based DA (RDA) method. We show the results for RDA-ADDA as the other DA variants, DANN and MMD, have similar performance. They are considered in the following real-world experiments (see Table 2). Finally, we observe in Figure 4 that DAF improves more significantly as the number of training samples becomes smaller.

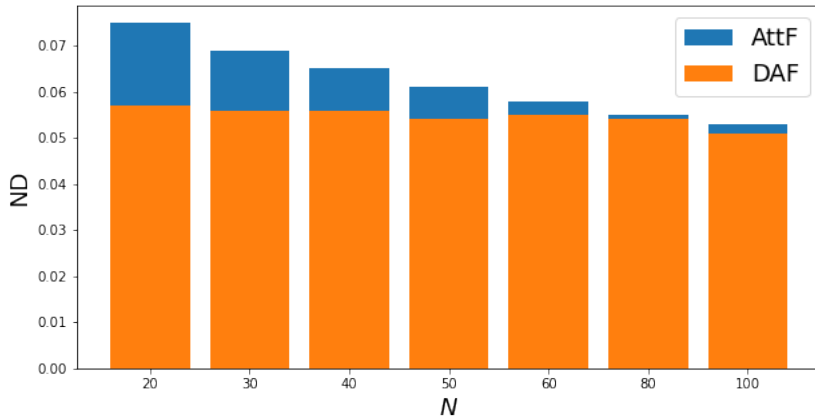


Figure 4: Forecasting accuracy of AttF and DAF methods in synthetic few-shot experiments with different target dataset sizes.

5.3 Real-World Datasets

| \mathcal{D}_T | \mathcal{D}_S | τ | DAR | VT | AttF | DATSING | RDA-DANN | RDA-ADDA | RDA-MMD | DAF |
|-----------------|-----------------|--------|-------------|-------------|-------------|-------------|-------------|--------------------|--------------------|--------------------|
| <i>traf</i> | <i>elec</i> | 24 | 0.205±0.015 | 0.187±0.003 | 0.182±0.007 | 0.184±0.004 | 0.181±0.009 | 0.174±0.005 | 0.186±0.004 | 0.169±0.002 |
| | <i>wiki</i> | | | | | 0.189±0.005 | 0.180±0.004 | 0.181±0.003 | 0.179±0.004 | 0.176±0.004 |
| <i>elec</i> | <i>traf</i> | 24 | 0.141±0.023 | 0.144±0.004 | 0.137±0.005 | 0.137±0.003 | 0.133±0.005 | 0.134±0.002 | 0.140±0.006 | 0.125±0.008 |
| | <i>sales</i> | | | | | 0.149±0.009 | 0.135±0.007 | 0.142±0.003 | 0.144±0.003 | 0.123±0.005 |
| <i>wiki</i> | <i>sales</i> | 7 | 0.055±0.010 | 0.061±0.008 | 0.050±0.003 | 0.049±0.002 | 0.047±0.005 | 0.045±0.003 | 0.045±0.003 | 0.042±0.004 |
| | <i>traf</i> | | | | | 0.052±0.004 | 0.053±0.002 | 0.049±0.003 | 0.052±0.004 | 0.049±0.003 |
| <i>sales</i> | <i>wiki</i> | 7 | 0.305±0.005 | 0.293±0.005 | 0.308±0.002 | 0.301±0.008 | 0.297±0.004 | 0.281±0.001 | 0.291±0.004 | 0.277±0.005 |
| | <i>elec</i> | | | | | 0.305±0.008 | 0.287±0.009 | 0.287±0.002 | 0.289±0.003 | 0.280±0.007 |

Table 2: Performance comparison of DAF on real-world benchmark datasets with prediction length τ in the target domain in terms of the mean \pm standard deviation ND metric. The winners and the competitive followers (the gap is smaller than its standard deviation over 5 runs) are bolded for reference.

| \mathcal{D}_T | \mathcal{D}_S | τ | <i>no-adv</i> | <i>no-q-share</i> | <i>no-k-share</i> | <i>v-share</i> | DAF |
|-----------------|-----------------|--------|---------------|-------------------|-------------------|----------------|--------------|
| <i>traf</i> | <i>elec</i> | 24 | 0.172 | 0.171 | 0.172 | 0.176 | 0.168 |
| <i>elec</i> | <i>traf</i> | 24 | 0.121 | 0.122 | 0.120 | 0.127 | 0.119 |
| <i>wiki</i> | <i>sales</i> | 7 | 0.042 | 0.042 | 0.044 | 0.049 | 0.041 |
| <i>sales</i> | <i>wiki</i> | 7 | 0.294 | 0.283 | 0.282 | 0.291 | 0.280 |

Figure 5: Results of ablation studies of DAF variants on four adaptation tasks on real-world datasets.

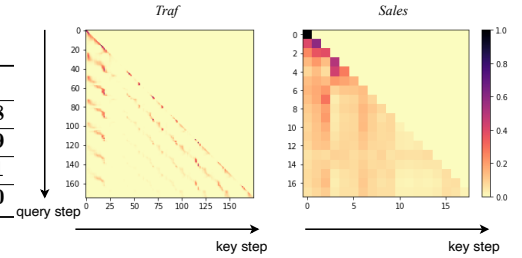


Figure 6: Attention distribution produced by an attention head of DAF with $\mathcal{D}_S = \textit{traf}$ (left) and $\mathcal{D}_T = \textit{sales}$ (right).

We perform experiments on four real benchmark datasets that are widely used in forecasting literature: *elec* and *traf* from the UCI data repository [Dua and Graff, 2017], *sales* [Kar, 2019] and *wiki* [Lai, 2017] from Kaggle. Notably, the *elec* and *traf* datasets present clear daily and weekly patterns while *sales* and *wiki* are less regular and more challenging. We use the following time features $\xi_t \in \mathbb{R}^2$ as covariates: the day of the week and hour of the day for the hourly datasets *elec* and *traf*, and the day of the month and day of the week for the daily datasets *sales* and *wiki*. For more dataset details, see appendix B.

To evaluate the performance of DAF, we consider cross-dataset adaptation, i.e., transferring between a pair of datasets. Since the original datasets are large enough to train a reasonably good forecaster, we only take a subset of each dataset as a target domain to simulate the data-scarce situation. Specifically, we take the last 30 days of each time series in the hourly dataset *elec* and *traf*, and the last 60 days from daily dataset *sales* and *wiki*. We partition the target datasets equally into training/validation/test splits, i.e. 10/10/10 days for hourly datasets and 20/20/20 days for daily datasets. The full datasets are used as source domains in adaptation. We follow the rolling window strategy from Flunkert et al. [2020], and split each window into historical and prediction time series of lengths T and $T + \tau$, respectively. In our experiments, we set $T = 168, \tau = 24$ for hourly datasets, and $T = 28, \tau = 7$ for the daily datasets. For DA methods, the splitting of the source data follows analogously.

Table 2 shows that the conclusions drawn from Table 1 on the synthetic experiments generally hold on the real-world datasets. In particular, we see the accuracy improvement by DAF over the baselines is more significant than that in the synthetic experiments. The real-world experiments also demonstrate that in general the success of DAF is agnostic of the source domain, and is even effective when transferring from a source domain of different frequency than that of the target domain. In addition, the cross-domain forecasters, DATSING, the RDA variants and our DAF outperform the three single-domain baselines in most cases. As in the synthetic cases, DATSING performs relatively worse than RDA and DAF. The accuracy differences between DAF and RDA are larger than in the synthetic case, and in favor of DAF. This finding further demonstrates that our choice of an attention-based architecture is well-suited for real domain adaptation problems.

Remarkably, DAF manages to learn the different patterns between source and target domains under our setups. For instance, Figure 6 illustrates that DAF can successfully learn clear daily patterns in the *traf* dataset, and find irregular patterns in the *sales* dataset. A reason for its success is that the private encoders capture features at various scales in different domains, and the attention module captures domain-dependent patterns by context matching using domain-invariant queries and keys.

5.4 Additional Experiments

In addition to the listed baselines in section 5.1, we also compare DAF with other single-domain forecasters, e.g. ConvTrans Li et al. [2019], N-BEATS Oreshkin et al. [2020a], and domain adaptation methods on time series tasks, e.g. MetaF Oreshkin et al. [2020b], Cai et al. [2021]. These methods are either similar to the baselines in Table 2 or designed for a different setting. We still adapt them to our setting to provide additional results in Tables 5-6 in appendix D, which further demonstrate that DAF outperforms the baselines in most cases.

5.5 Ablation Studies

In order to examine the effectiveness of our designs, we conduct ablation studies by adjusting each key component successively. Table 5 shows the improved performance of DAF over its variants on the target domain on four adaptation tasks. Equipped with a domain discriminator, DAF improves its effectiveness of adaptation compared to its non-adversarial variant (*no-adv*). We see that sharing both keys and queries in DAF results in performance gains over not sharing either (*no-k-share* and *no-q-share*). Furthermore, it is clear that our design choice of the values to be domain-specific for domain-dependent forecasts rather than shared (*v-share*) has the largest positive impact on the performance.

Figure 7 visualizes the distribution of queries and keys learned by DAF and *no-adv*, where the target data $\mathcal{D}_T = \text{traf}$ and the source data $\mathcal{D}_S = \text{elec}$ via a TSNE embedding. Empirically, we see the latent distributions are well aligned in DAF and not in *no-adv*. This can explain the improved performance of DAF over its variants. It also further verifies our intuition that DAF benefits from an aligned latent space of queries and keys across domains.

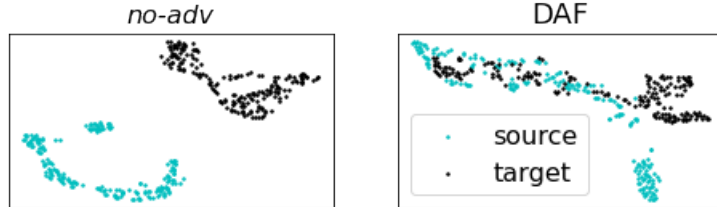


Figure 7: Query alignment with (DAF: right) and without adversarial training (*no-adv*: left), where $\mathcal{D}_S = \text{elec}$ and $\mathcal{D}_T = \text{traf}$.

6 Conclusions

In this paper, we aim to apply domain adaptation to time series forecasting to solve the data scarcity problem. We identify the differences between the forecasting task and common domain adaptation scenarios, and accordingly propose the Domain Adaptation Forecaster (DAF) based on attention sharing. Through empirical experiments, we demonstrate that DAF outperforms state-of-the-art single-domain forecasters and various domain adaptation baselines on synthetic and real-world datasets. We further show the effectiveness of our designs via extensive ablation studies. In spite of empirical evidences, the theoretical justification of having domain-invariant features within attention models remains an open problem. Extension to multi-variate time series forecasting experiments is another direction of future work.

References

- Valentin Flunkert, David Salinas, and Jan Gasthaus. DeepAR: Probabilistic Forecasting with Autoregressive Recurrent Networks. *International Journal of Forecasting*, 36:1181–1191, 2020. arXiv: 1704.04110.
- Anastasia Borovykh, Sander Bohte, and Cornelis W Oosterlee. Conditional time series forecasting with convolutional neural networks. *arXiv preprint arXiv:1703.04691*, 2017.
- Boris N Oreshkin, Nicolas Chapados, Dmitri Carпов, and Yoshua Bengio. N-BEATS: Neural basis expansion analysis for interpretable time series forecasting. *International Conference on Learning Representations*, page 31, 2020a.
- Youngsuk Park, Danielle Maddix, François-Xavier Aubet, Kelvin Kan, Jan Gasthaus, and Yuyang Wang. Learning Quantile Functions without Quantile Crossing for Distribution-free Time Series Forecasting, 2021. _eprint: 2111.06581.
- Ashish Vaswani, Noam Shazeer, Niki Parmar, Jakob Uszkoreit, Llion Jones, Aidan N. Gomez, Lukasz Kaiser, and Illia Polosukhin. Attention Is All You Need. In *Advances in neural information processing systems*, pages 5998–6008, 2017.
- Shiyang Li, Xiaoyong Jin, Yao Xuan, Xiyu Zhou, Wenhui Chen, Yu-Xiang Wang, and Xifeng Yan. Enhancing the Locality and Breaking the Memory Bottleneck of Transformer on Time Series Forecasting. *Advances in Neural Information Processing Systems*, pages 5243–5253, 2019.
- Bryan Lim, Sercan O. Arik, Nicolas Loeff, and Tomas Pfister. Temporal Fusion Transformers for Interpretable Multi-horizon Time Series Forecasting. *arXiv:1912.09363 [cs, stat]*, December 2019. URL <http://arxiv.org/abs/1912.09363>. arXiv: 1912.09363.
- Rui Wang, Danielle Maddix, Christos Faloutsos, Yuyang Wang, and Rose Yu. Bridging Physics-based and Data-driven modeling for Learning Dynamical Systems. In *Learning for Dynamics and Control*, pages 385–398, 2021.
- Yaroslav Ganin, Evgeniya Ustinova, Hana Ajakan, Pascal Germain, Hugo Larochelle, François Laviolette, Mario Marchand, and Victor Lempitsky. Domain-Adversarial Training of Neural Networks. *The journal of machine learning research*, 17:2096–2030, 2016.
- Konstantinos Bousmalis, George Trigeorgis, Nathan Silberman, Dilip Krishnan, and Dumitru Erhan. Domain Separation Networks. volume 29, pages 345–351, 2016.
- Judy Hoffman, Eric Tzeng, Taesung Park, Jun-Yan Zhu, Phillip Isola, Kate Saenko, Alexei A Efros, and Trevor Darrell. CyCADA: Cycle-Consistent Adversarial Domain Adaptation. *International conference on machine learning*, pages 1989–1998, 2018.
- Sergey Bartunov and Dmitry P Vetrov. Few-shot Generative Modelling with Generative Matching Networks. *International Conference on Artificial Intelligence and Statistics*, pages 670–678, 2018.
- Garrett Wilson and Diane J. Cook. A Survey of Unsupervised Deep Domain Adaptation. *arXiv:1812.02849 [cs, stat]*, February 2020. URL <http://arxiv.org/abs/1812.02849>. arXiv: 1812.02849.
- Ruofeng Wen, Kari Torkkola, Balakrishnan Narayanaswamy, and Dhruv Madeka. A Multi-Horizon Quantile Recurrent Forecaster. *arXiv:1711.11053 [stat]*, November 2017. URL <http://arxiv.org/abs/1711.11053>. arXiv: 1711.11053.
- Yuyang Wang, Alex Smola, Danielle C Maddix, Jan Gasthaus, Dean Foster, and Tim Januschowski. Deep Factors for Forecasting. In *International conference on machine learning*, pages 6607–6617, 2019.
- Rajat Sen, Hsiang-Fu Yu, and Inderjit Dhillon. Think Globally, Act Locally: A Deep Neural Network Approach to High-Dimensional Time Series Forecasting. *Advances in Neural Information Processing Systems*, 32, 2019.

- Syama Sundar Rangapuram, Matthias Seeger, Jan Gasthaus, Lorenzo Stella, Yuyang Wang, and Tim Januschowski. Deep State Space Models for Time Series Forecasting. In *Advances in neural information processing systems*, pages 7785–7794, 2018.
- Sifan Wu, Xi Xiao, Qianggang Ding, Peilin Zhao, Ying Wei, and Junzhou Huang. Adversarial Sparse Transformer for Time Series Forecasting. *Advances in Neural Information Processing Systems*, 33:11, 2020.
- Haoyi Zhou, Shanghang Zhang, Jieqi Peng, Shuai Zhang, Jianxin Li, Hui Xiong, and Wancai Zhang. Informer: Beyond Efficient Transformer for Long Sequence Time-Series Forecasting. In *Proceedings of the AAAI Conference on Artificial Intelligence*, 2021. URL <http://arxiv.org/abs/2012.07436>. arXiv: 2012.07436.
- Wen Wang, Pieter HAJM Van Gelder, and JK Vrijling. Some issues about the generalization of neural networks for time series prediction. In *International Conference on Artificial Neural Networks*, pages 559–564. Springer, 2005.
- Sanjay Purushotham, Wilka Carvalho, Tanachat Nilanon, and Yan Liu. Variational Recurrent Adversarial Deep Domain Adaptation. In *5th International Conference on Learning Representations, ICLR 2017, Toulon, France, April 24-26, 2017, Conference Track Proceedings*. OpenReview.net, 2017. URL <https://openreview.net/forum?id=rk9eAFcxg>.
- Saeid Motiian, Quinn Jones, Seyed Mehdi Iranmanesh, and Gianfranco Doretto. Few-Shot Adversarial Domain Adaptation. *Advances in Neural Information Processing Systems*, pages 6670–6680, 2017. URL <http://arxiv.org/abs/1711.02536>. arXiv: 1711.02536.
- Alan Ramponi and Barbara Plank. Neural Unsupervised Domain Adaptation in NLP—A Survey. *arXiv:2006.00632 [cs]*, May 2020. URL <http://arxiv.org/abs/2006.00632>. arXiv: 2006.00632.
- Jacob Devlin, Ming-Wei Chang, Kenton Lee, and Kristina Toutanova. BERT: Pre-training of Deep Bidirectional Transformers for Language Understanding. In *Proceedings of the 2019 Conference of the North American Chapter of the Association for Computational Linguistics: Human Language Technologies, Volume 1 (Long and Short Papers)*, pages 4171–4186, 2019. URL <http://arxiv.org/abs/1810.04805>. arXiv: 1810.04805.
- Xiaochuang Han and Jacob Eisenstein. Unsupervised Domain Adaptation of Contextualized Embeddings for Sequence Labeling. In *Proceedings of the 2019 Conference on Empirical Methods in Natural Language Processing and the 9th International Joint Conference on Natural Language Processing (EMNLP-IJCNLP)*, pages 4237–4247, Hong Kong, China, 2019. Association for Computational Linguistics. doi:10.18653/v1/D19-1433. URL <https://www.aclweb.org/anthology/D19-1433>.
- Suchin Gururangan, Ana Marasović, Swabha Swayamdipta, Kyle Lo, Iz Beltagy, Doug Downey, and Noah A. Smith. Don’t Stop Pretraining: Adapt Language Models to Domains and Tasks. In *Proceedings of the 58th Annual Meeting of the Association for Computational Linguistics*, pages 8342–8360, Online, 2020. Association for Computational Linguistics. doi:10.18653/v1/2020.acl-main.740. URL <https://www.aclweb.org/anthology/2020.acl-main.740>.
- Alexander Rietzler, Sebastian Stabinger, Paul Opitz, and Stefan Engl. Adapt or Get Left Behind: Domain Adaptation through BERT Language Model Finetuning for Aspect-Target Sentiment Classification. *Proceedings of The 12th Language Resources and Evaluation Conference*, pages 4933–4941, 2020.
- Shai Ben-David, John Blitzer, Koby Crammer, Alex Kulesza, Fernando Pereira, and Jennifer Wortman Vaughan. A theory of learning from different domains. *Machine Learning*, 79(1-2):151–175, May 2010. ISSN 0885-6125, 1573-0565. doi:10.1007/s10994-009-5152-4. URL <http://link.springer.com/10.1007/s10994-009-5152-4>.
- Corinna Cortes and Mehryar Mohri. Domain Adaptation in Regression. In Jyrki Kivinen, Csaba Szepesvári, Esko Ukkonen, and Thomas Zeugmann, editors, *Algorithmic Learning Theory*, volume 6925, pages 308–323. Springer Berlin Heidelberg, Berlin, Heidelberg, 2011. ISBN 978-3-642-24411-7 978-3-642-24412-4. doi:10.1007/978-3-642-24412-4_25. URL http://link.springer.com/10.1007/978-3-642-24412-4_25. Series Title: Lecture Notes in Computer Science.

- Yaroslav Ganin and Victor Lempitsky. Unsupervised Domain Adaptation by Backpropagation. *International conference on machine learning*, pages 1180–1189, 2015.
- Eric Tzeng, Judy Hoffman, Kate Saenko, and Trevor Darrell. Adversarial Discriminative Domain Adaptation. In *2017 IEEE Conference on Computer Vision and Pattern Recognition (CVPR)*, pages 2962–2971, Honolulu, HI, July 2017. IEEE. ISBN 978-1-5386-0457-1. doi:10.1109/CVPR.2017.316. URL <http://ieeexplore.ieee.org/document/8099799/>.
- Han Zhao, Shanghang Zhang, Guanhong Wu, José M F Moura, Joao P Costeira, and Geoffrey J Gordon. Adversarial Multiple Source Domain Adaptation. *Advances in neural information processing systems*, pages 8559–8570, 2018.
- Firoj Alam, Shafiq Joty, and Muhammad Imran. Domain Adaptation with Adversarial Training and Graph Embeddings. In *Proceedings of the 56th Annual Meeting of the Association for Computational Linguistics (Volume 1: Long Papers)*, pages 1077–1087, Melbourne, Australia, 2018. Association for Computational Linguistics. doi:10.18653/v1/P18-1099. URL <http://aclweb.org/anthology/P18-1099>.
- Dustin Wright and Isabelle Augenstein. Transformer Based Multi-Source Domain Adaptation. In *Proceedings of the 2020 Conference on Empirical Methods in Natural Language Processing (EMNLP)*, pages 7963–7974, Online, 2020. Association for Computational Linguistics. doi:10.18653/v1/2020.emnlp-main.639. URL <https://www.aclweb.org/anthology/2020.emnlp-main.639>.
- Mingsheng Long, Yue Cao, Jianmin Wang, and Michael I. Jordan. Learning Transferable Features with Deep Adaptation Networks. pages 97–105, 2015. URL <http://arxiv.org/abs/1502.02791>. arXiv: 1502.02791.
- Wei-Yu Chen, Yen-Cheng Liu, Zsolt Kira, Yu-Chiang Frank Wang, and Jia-Bin Huang. A Closer Look at Few-shot Classification. *arXiv:1904.04232 [cs]*, January 2020. URL <http://arxiv.org/abs/1904.04232>. arXiv: 1904.04232.
- Han Guo, Ramakanth Pasunuru, and Mohit Bansal. Multi-Source Domain Adaptation for Text Classification via DistanceNet-Bandits. *Proceedings of the AAAI Conference on Artificial Intelligence*, 34(05):7830–7838, April 2020. ISSN 2374-3468, 2159-5399. doi:10.1609/aaai.v34i05.6288. URL <https://aaai.org/ojs/index.php/AAAI/article/view/6288>.
- Garrett Wilson, Janardhan Rao Doppa, and Diane J. Cook. Multi-Source Deep Domain Adaptation with Weak Supervision for Time-Series Sensor Data. In *Proceedings of the 26th ACM SIGKDD International Conference on Knowledge Discovery & Data Mining*, pages 1768–1778, Virtual Event CA USA, August 2020. ACM. ISBN 978-1-4503-7998-4. doi:10.1145/3394486.3403228. URL <https://dl.acm.org/doi/10.1145/3394486.3403228>.
- Ruichu Cai, Jiawei Chen, Zijian Li, Wei Chen, Keli Zhang, Junjian Ye, Zhuozhang Li, Xiaoyan Yang, and Zhenjie Zhang. Time Series Domain Adaptation via Sparse Associative Structure Alignment. *Proceedings of the AAAI Conference on Artificial Intelligence*, 35:6859–6867, 2021.
- Hailin Hu, MingJian Tang, and Chengcheng Bai. DATSING: Data Augmented Time Series Forecasting with Adversarial Domain Adaptation. In *Proceedings of the 29th ACM International Conference on Information & Knowledge Management*, pages 2061–2064, Virtual Event Ireland, October 2020. ACM. ISBN 978-1-4503-6859-9. doi:10.1145/3340531.3412155. URL <https://dl.acm.org/doi/10.1145/3340531.3412155>.
- Muhammad Ghifary, W. Bastiaan Kleijn, Mengjie Zhang, David Balduzzi, and Wen Li. Deep Reconstruction-Classification Networks for Unsupervised Domain Adaptation. In *European conference on computer vision*, pages 597–613, 2016.
- Ge Shi, Chong Feng, Lifu Huang, Boliang Zhang, Heng Ji, Lejian Liao, and Heyan Huang. Genre Separation Network with Adversarial Training for Cross-genre Relation Extraction. In *Proceedings of the 2018 Conference on Empirical Methods in Natural Language Processing*, pages 1018–1023, Brussels, Belgium, 2018. Association for Computational Linguistics. doi:10.18653/v1/D18-1125. URL <http://aclweb.org/anthology/D18-1125>.

- Chun-Liang Li, Wei-Cheng Chang, Yu Cheng, Yiming Yang, and Barnabás Póczos. MMD GAN: towards deeper understanding of moment matching network. In *Proceedings of the 31st International Conference on Neural Information Processing Systems*, pages 2200–2210, 2017.
- Adam Paszke, Sam Gross, Francisco Massa, Adam Lerer, James Bradbury, Gregory Chanan, Trevor Killeen, Zeming Lin, Natalia Gimelshein, Luca Antiga, Alban Desmaison, Andreas Kopf, Edward Yang, Zachary DeVito, Martin Raison, Alykhan Tejani, Sasank Chilamkurthy, Benoit Steiner, Lu Fang, Junjie Bai, and Soumith Chintala. PyTorch: An Imperative Style, High-Performance Deep Learning Library. *Advances in neural information processing systems*, pages 8026–8037, 2019.
- Edo Liberty, Zohar Karnin, Bing Xiang, Laurence Rouesnel, Baris Coskun, Ramesh Nallapati, Julio Delgado, Amir Sadoughi, Yury Astashonok, Piali Das, Can Balioglu, Saswata Chakravarty, Madhav Jha, Philip Gautier, David Arpin, Tim Januschowski, Valentin Flunkert, Yuyang Wang, Jan Gasthaus, Lorenzo Stella, Syama Rangapuram, David Salinas, Sebastian Schelter, and Alex Smola. Elastic Machine Learning Algorithms in Amazon SageMaker. In *Proceedings of the 2020 ACM SIGMOD International Conference on Management of Data*, pages 731–737, Portland OR USA, June 2020. ACM. ISBN 978-1-4503-6735-6. doi:10.1145/3318464.3386126. URL <https://dl.acm.org/doi/10.1145/3318464.3386126>.
- Hsiang-Fu Yu, Nikhil Rao, and Inderjit S Dhillon. Temporal Regularized Matrix Factorization for High-dimensional Time Series Prediction. *NIPS*, pages 847–855, 2016.
- Dheeru Dua and Casey Graff. *UCI Machine Learning Repository*. University of California, Irvine, School of Information and Computer Sciences, 2017. URL <http://archive.ics.uci.edu/ml>.
- Pratyusha Kar. Dataset of Kaggle Competition Rossmann Store Sales, version 2, January 2019. URL <https://www.kaggle.com/pratyushakar/rossmann-store-sales>.
- Lai. Dataset of Kaggle Competition Web Traffic Time Series Forecasting, Version 3, August 2017. URL <https://www.kaggle.com/ymlai87416/wiktraffictimeseriesforecast/metadata>.
- Boris N. Oreshkin, Dmitri Carpov, Nicolas Chapados, and Yoshua Bengio. Meta-learning framework with applications to zero-shot time-series forecasting. *arXiv:2002.02887 [cs, stat]*, February 2020b. URL <http://arxiv.org/abs/2002.02887>. arXiv: 2002.02887.
- Marco Cuturi and Mathieu Blondel. Soft-DTW: a Differentiable Loss Function for Time-Series. *arXiv:1703.01541 [stat]*, March 2017. URL <http://arxiv.org/abs/1703.01541>. arXiv: 1703.01541.

A Attention module

The attention module in our proposed Domain Adaptation Forecaster (DAF) model performs input reconstruction (interpolation) and future prediction (extrapolation) using the same set of queries, keys and values. It uses different choices of neighborhood positions $\mathcal{N}(t)$ and position translations $\mu(t)$, as mentioned in section 4.1. The queries $\mathbf{Q} = [\mathbf{q}_t]_{t=1}^T$ and keys $\mathbf{K} = [\mathbf{k}_t]_{t=1}^T$ are dependent on the pattern embeddings produced by the convolutional layers in the encoder module, which encode a local window of raw time series. The specific settings of $\mathcal{N}(t)$ and $\mu(t)$ depend on the kernel sizes s of the involved convolutions. Figure 8(a) illustrates and example architecture with the number of convolutions $M = 1$ and kernel sizes $s = 3$.

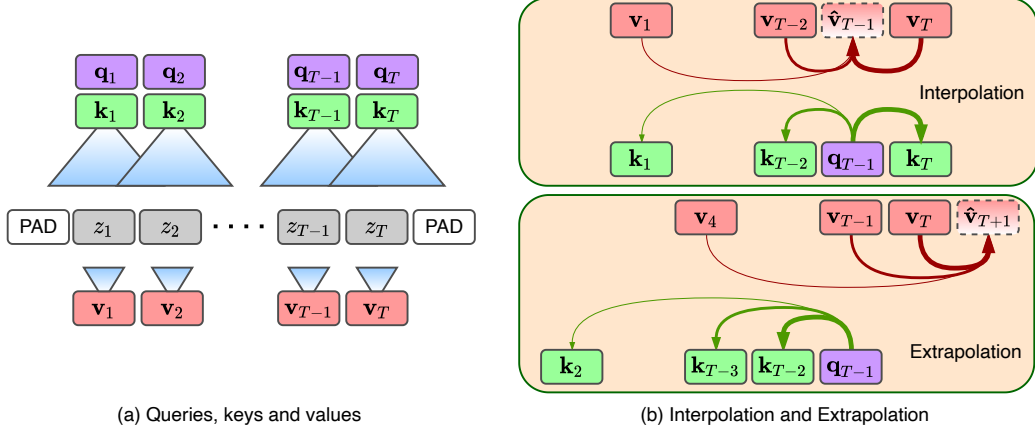


Figure 8: Interpolation and extrapolation within an attention module where $s = 3$ and $M = 1$. Specifically, the lower panel of (b) describes how attention is performed to estimate \mathbf{v}_{T+1} . The extrapolation query q_{T+1} comes from the last local window z_{T-2}, z_{T-1}, z_T , which is convoluted into q_{T-1} . Meanwhile, a key $k_{t'}$ comes from the window $z_{t'-1}, z_{t'}, z_{t'+1}$ via convolution. Since the predicted z_{T+1} follows the query window z_{T-2}, z_{T-1}, z_T , we take the value that follows the key window $z_{t'-1}, z_{t'}, z_{t'+1}$, i.e. $z_{t'+2}$, to make a correspondence. In this way, the following value of similar windows to the query window will receive larger weights in attention. For example, in Figure 7, the key k_{T-2} corresponds to the value v_T , where the correspondence is indicated by the boldness of the arrows. Therefore, the key $k_{t'}$ will be paired with the value $v_{t'+s+1}$, and $\mu(t') = t' + s + 1$.

Interpolation: Input Reconstruction We reconstruct the input by interpolating \hat{z}_t using the observations at other time points. The upper panel of Figure 8(b) illustrates an example, where we would like to estimate \hat{z}_{T-1} using $\{z_1, z_2, \dots, z_{T-2}, z_T\}$. We take \mathbf{q}_{T-1} that depends on the local windows centered at the target step $T - 1$ as shown in Figure 8(a) as the query, and compare it with the keys $\{\mathbf{k}_1, \mathbf{k}_2, \dots, \mathbf{k}_{T-2}, \mathbf{k}_T\}$. The attention scores $\alpha(\mathbf{q}_{T-1}, \mathbf{k}_{t'})$ are computed by comparison using equation (5), and illustrated by the thickness of arrows in Figure 8(b). Similar to the query, the attended keys $\mathbf{k}_{t'}$ depend on local windows centered at the respective step t' . Hence, the scores $\alpha(\mathbf{q}_{T-1}, \mathbf{k}_{t'})$ depict the similarity of the value \hat{z}_{T-1} to the attended value $z_{t'}$, and we compute the output \mathbf{o}_{T-1} based on the combination of $\mathbf{v}_{t'}$ weighted by $\alpha(\mathbf{q}_{T-1}, \mathbf{k}_{t'})$ according to equation (5).

To generalize the example at time $T - 1$ in Figure 8(b), we formally set

$$\begin{aligned}\mathcal{N}(t) &= \{1, 2, \dots, T\} \setminus \{t\}, \\ \mu(t') &= t',\end{aligned}$$

in equation (6). Although the ground truth z_t is encoded in the query, and the nearby keys within the local window are centered at time step t , it is not incorporated in \mathbf{o}_t , which instead depends on values at $\mathcal{N}(t)$.

Extrapolation: Future Predictions Since DAF is an autoregressive forecaster, it generates forecasts one step ahead. At each step, we forecast the next value by extrapolating from the given historical values. The

lower panel of Figure 8(b) illustrates an example, where we would like to estimate the $(T+1)$ -th value given the past T observations and expected. The prediction \hat{z}_{T+1} follows the last local window $\{z_{T-s+1}, z_{T-s+2}, \dots, z_T\}$ on which the query $\mathbf{q}_{T-\bar{s}}$ is dependent, where $\bar{s} = \lceil \frac{s-1}{2} \rceil$, and $\lceil \cdot \rceil$ denotes the ceiling operator. We take $\mathbf{q}_{T-\bar{s}}$ as the query for $T+1$, i.e. we set $\mathbf{q}_{T+1} = \mathbf{q}_{T-\bar{s}}$, and attend to the previous keys that do not encode padding zeros, i.e. we set:

$$\mathcal{N}(T+1) = \{s, \dots, T - \bar{s} - 1\}.$$

In this case, the attention score $\alpha(\mathbf{q}_{T+1}, \mathbf{k}_{t'})$ from equation (5) depicts the similarity of the unknown \hat{z}_{T+1} , and the value $z_{t'+\bar{s}+1}$ following the local window $\{z_{t'-\bar{s}}, \dots, z_{t'}, \dots, z_{t'+\bar{s}}\}$ corresponding to the attended key $\mathbf{k}_{t'}$. Hence, we set

$$\mu(t') = t' + \bar{s} + 1,$$

in equation (6) to estimate \mathbf{o}_{T+1} .

Figure 8 illustrates an example of future forecasts, where $s = 3$ and $M = 1$ in encoder module. A detailed walkthrough of can be found in the caption.

B Dataset Details

B.1 Synthetic Datasets

The synthetic datasets consist of sinusoidal signals with uniformly sampled parameters as follows:

$$\begin{aligned} z_{i,t} &= A_i \sin(2\pi\omega_i t + \phi_i) + c_i + \epsilon_{i,t}, \quad t \in [0, T + \tau], \\ A_i &\sim \text{Unif}(A_{\min}, A_{\max}), \quad c_i \sim \text{Unif}(c_{\min}, c_{\max}), \\ \omega_i &\sim \text{Unif}(\omega_{\min}, \omega_{\max}), \quad \phi_i \sim \text{Unif}(-2\pi, 2\pi), \end{aligned}$$

where $A_{\min}, A_{\max} \in \mathbb{R}^+$ denote the amplitudes, $c_{\min}, c_{\max} \in \mathbb{R}$ denote the levels, and $\omega_{\min}, \omega_{\max} \in [\frac{1}{T}, \frac{20}{T}]$ denote the frequencies. In addition, $\epsilon_{i,t} \sim \mathcal{N}(0, 0.2)$ is a white noise term. In our experiments, we fix $T = 144, \tau = 18, A_{\min} = 0.5, A_{\max} = 5.0, c_{\min} = -3.0, c_{\max} = 3.0$.

B.2 Real-World Datasets

Table 3 summarizes the four benchmark real-world datasets that we use to evaluate our DAF model.

| Dataset | Freq | Value | # Time Series | Average Length | Comment |
|--------------|--------|----------------|---------------|----------------|---|
| <i>elec</i> | hourly | \mathbb{R}^+ | 370 | 3304 | Household electricity consumption |
| <i>traf</i> | hourly | $[0, 1]$ | 963 | 360 | Occupancy rate of SF Bay Area highways |
| <i>sales</i> | daily | \mathbb{N}^+ | 500 | 1106 | Daily sales of Rossmann grocery stores |
| <i>wiki</i> | daily | \mathbb{N}^+ | 9906 | 70 | Visit counts of various Wikipedia pages |

Table 3: Benchmark dataset descriptions.

For evaluation, we follow Flunkert et al. [2020], and we take moving windows of length $T + \tau$ starting at different points from the original time series in the datasets. For an original time series $[z_{i,t}]_{t=1}^L$ of length L , we obtain a set of moving windows:

$$\{[z_{i,t}]_{t=n}^{n+T+\tau-1}, \quad n = 1, 2, \dots, L - T - \tau + 1\}.$$

This procedure results in a set of fixed-length trajectory samples. Each sample is further split into historical observations X and forecasting targets Y , where the lengths of X and Y are T and τ , respectively. We randomly select samples from the population by uniform sampling for training, validation and test sets.

C Implementation Details

C.1 Baselines

In this subsection, we provide an overview of the following baseline models, including conventional single-domain forecasters trained only on the target domain:

- DeepAR (DAR): auto-regressive RNN-based model with LSTM units (we directly call DeepAR implemented by Amazon Sagemaker);
- Vanilla Transformer (VT): sequence-to-sequence model based on common transformer architecture;
- ConvTrans (CT): attention-based forecaster that builds attention blocks on convolutional activations as DAF does. Unlike DAF, it does not reconstruct the input, and only fits the future. From a probabilistic perspective, it models the conditional distribution $P(Y|X)$ instead of the joint distribution $P(X, Y)$ as DAF does, where X and Y are history and future, respective. In addition, it directly uses the outputs of the convolution as queries and keys in the attention module;
- AttF: single-domain version of DAF. It is equivalent to the branch of the sequence generator for the target domain in DAF. It has access to the attention module, but does not share it with another branch;
- N-BEATS: MLP-based forecaster. Similar to DAF, it aims to forecast the future as well as to reconstruct the given history. N-BEATS only consumes univariate time series $z_{i,t}$, and does not accept covariates $\xi_{i,t}$ as input. In the original paper Oreshkin et al. [2020a], it employs various objectives and ensembles to improve the results. In our implementation, we use the ND metric as the training objective, and do not use any ensembling techniques for a fair comparison;

and cross-domain forecasters trained on both source and target domain:

- MetaF: method with the same architecture as N-BEATS. It trains a model on the source dataset, and applies it to the target dataset in a zero-shot setting, i.e. without any fine-tuning. Both MetaF and N-BEATS rely on given Fourier bases to fit seasonal patterns. For instance, bases of period 24 and 168 are included for hourly datasets, whereas bases of period 7 are included for daily datasets. The daily and weekly patterns are expected to be captured in all settings.
- PreTrained Forecaster (PTF): method with the same architecture as AttF for the target data. Unlike AttF, PTF fits both source and target data. It is first pretrained on the source dataset, and then finetuned on the target dataset.
- DATSING: a forecasting framework based on NBEATS Oreshkin et al. [2020a] architecture. The model is first pre-trained on the source dataset. Then a subset of source data that includes nearest neighbors to a target sample in terms of soft-DTW Cuturi and Blondel [2017] is selected to fine-tune the pre-trained model before it is evaluated using the respective target sample. During fine-tuning, a domain discriminator is used to distinguish the nearest neighbors from the same number of source samples drawn from the complement set.
- RDA has the same overall structure as DAF, but replaces the attention module in DAF with a LSTM module. The encoder module produces a single encoding, which is then consumed by the MLP-based decoder. We take three traditional methods for domain adaptation:
 - RDA-DANN: The encoder and decoder are shared across domains. The sequence generator is trained to fit data from both domains. Meanwhile, the gradient of domain discriminator will be reversed before back-propagated to the encoder.
 - RDA-ADDF: The encoder and decoder are not shared across domains. During training, the source encoder and decoder are first trained to fit source data. Then encodings from both encoders are discriminated by the domain discriminator with the source encoder parameters frozen. Finally, the target encoder and decoder are trained to fit target data with the target encoder parameters frozen.
 - RDA-MMD: Instead of a domain discriminators, the Maximum Mean Discrepancy between source and target encodings is optimized with the sequence generators.

C.2 Hyperparameters

The following hyperparameters of DAF and baseline models are selected by grid-search over the validation set:

- the hidden dimension $h \in \{32, 64, 128, 256\}$ of all models;
- the number of MLP layers $l_{\text{MLP}} \in \{4\}$ for N-BEATS ¹, $l_{\text{MLP}} \in \{1, 2, 3\}$ for AttF, DAF and its variants;
- the number of RNN layers $l_{\text{RNN}} \in \{1, 3\}$ in DAR and RDA;
- the kernel sizes of convolutions $s \in \{3, 13, (3, 5), (3, 17)\}$ in AttF, DAF and its variants; ²
- the learning rate $\gamma \in \{0.001, 0.01, 0.1\}$ for all models;
- the trade-off coefficient $\lambda \in \{0.1, 1, 10\}$ in equation (2) for DAF, RDA-ADDA;
- In RDA-MMD, the factor of the MMD item in the objective selected from $\{0.1, 1.0, 10.0\}$.

For RDA-DANN, we set a schedule

$$\lambda = \frac{2}{1 + \exp(-10e/E)} - 1,$$

where e denotes the current epoch and E denotes the total number of epochs for the factor λ of the reversed gradient from the domain discriminator according to Ganin et al. [2016].

Table 4 summarizes the specific configurations of the hyper-parameters for our proposed DAF model in the experiments.

| | h | l_{MLP} | s | γ | λ |
|--------------|-----|------------------|--------|----------|-----------|
| cold-start | 64 | 1 | (3,5) | 1e-3 | 1.0 |
| few-shot | | | | | |
| <i>elec</i> | 128 | 1 | 13 | 1e-3 | 1.0 |
| <i>traf</i> | 64 | 1 | (3,17) | 1e-2 | 10.0 |
| <i>wiki</i> | 64 | 2 | (3,5) | 1e-3 | 1.0 |
| <i>sales</i> | 128 | 2 | (3,5) | 1e-3 | 1.0 |

Table 4: Hyperparameters of DAF models in various synthetic and real-world experiments.

The models are trained for at most 100K iterations, which we empirically find to be more than sufficient for the models to converge. We use early stopping with respect to the ND metric on the validation set.

D Detailed Experiment Results

Tables 5-6 display a comprehensive comparison of DAF with all the aforementioned baselines on the synthetic and real-world data, respectively. As a conclusion, we see that DAF outperforms or is on par with the baselines in all cases with RDA-ADDA being the most competitive in some cases.

Cai et al. [2021] is another related work that we introduce in section 2, which focuses on time series classification and regression tasks, where a single exogenous label instead of a sequence of future values is predicted. Although it can be adapted to the multi-horizon forecasting by autoregressively predicting the next step, the model takes a fixed number of historical inputs at each time step, which makes its comparison with DAF that can access the entire history unfair. Therefore, we provide a comparison under a one-step ahead forecasting scenario. In other words, we replace the original labels of the regression task with the next value of the respective time series for Cai et al. [2021], and set the forecasting horizon of DAF to be 1. In the experiments, we use the official code ³ of Cai et al. [2021] with the provided default hyperparameters. Table 7 shows that our method is better in a majority (6/8) of test cases with a maximum accuracy improvement of approximately 18% as expected, since it is explicitly designed for the forecasting task.

¹ We set the other hyperparameters for N-BEATS as suggested in the original paper Oreshkin et al. [2020a]. ² A single integer means a single convolution layer in the encoder module, while a tuple stands for multiple convolutions.

³ <https://github.com/DMIRLAB-Group/SASA>.

| Task | Cold-start | | | Few-shot | | |
|----------|--------------------|--------------------|--------------------|--------------------|--------------------|--------------------|
| N | 5000 | | | 20 | 50 | 100 |
| T | 36 | 45 | 54 | 144 | | |
| τ | 18 | | | | | |
| DeepAR | 0.053±0.003 | 0.037±0.002 | 0.031±0.002 | 0.062±0.003 | 0.059±0.004 | 0.059±0.003 |
| N-BEATS | 0.044±0.001 | 0.044±0.001 | 0.042±0.001 | 0.079±0.001 | 0.060±0.001 | 0.054±0.002 |
| CT | 0.042±0.001 | 0.041±0.004 | 0.038±0.005 | 0.095±0.003 | 0.074±0.005 | 0.071±0.002 |
| AttF | 0.042±0.001 | 0.041±0.004 | 0.038±0.005 | 0.095±0.003 | 0.074±0.005 | 0.071±0.002 |
| MetaF | 0.045±0.005 | 0.043±0.006 | 0.042±0.002 | 0.071±0.004 | 0.061±0.003 | 0.053±0.003 |
| PTF | 0.039±0.006 | 0.037±0.005 | 0.034±0.008 | 0.086±0.004 | 0.086±0.003 | 0.081±0.005 |
| DATSING | 0.039±0.004 | 0.039±0.002 | 0.037±0.001 | 0.078±0.005 | 0.076±0.006 | 0.058±0.005 |
| RDA-ADDA | 0.035±0.002 | 0.034±0.001 | 0.034±0.001 | 0.059±0.003 | 0.054±0.003 | 0.053±0.007 |
| DAF | 0.035±0.003 | 0.030±0.003 | 0.029±0.003 | 0.057±0.004 | 0.055±0.001 | 0.051±0.001 |

Table 5: Performance comparison of DAF to all baselines on synthetic datasets. The winners and the competitive followers (the gap is smaller than its standard deviation over 5 runs) are bolded for reference.

| \mathcal{D}_T | <i>traf</i> | | <i>elec</i> | | <i>wiki</i> | | <i>sales</i> | |
|-----------------|--------------------|--------------------|--------------------|--------------------|--------------------|--------------------|--------------------|--------------------|
| \mathcal{D}_S | <i>elec</i> | <i>wiki</i> | <i>traf</i> | <i>sales</i> | <i>elec</i> | <i>sales</i> | <i>traf</i> | <i>wiki</i> |
| DAR | 0.205±0.015 | | 0.141±0.023 | | 0.055±0.010 | | 0.305±0.005 | |
| N-BEATS | 0.191±0.003 | | 0.147±0.004 | | 0.059±0.008 | | 0.299±0.005 | |
| VT | 0.187±0.003 | | 0.144±0.004 | | 0.061±0.008 | | 0.293±0.005 | |
| CT | 0.183±0.013 | | 0.131±0.005 | | 0.051±0.006 | | 0.324±0.013 | |
| AttF | 0.182±0.007 | | 0.137±0.005 | | 0.050±0.003 | | 0.308±0.002 | |
| MetaF | 0.190±0.005 | 0.188±0.002 | 0.151±0.004 | 0.144±0.004 | 0.061±0.003 | 0.059±0.005 | 0.311±0.001 | 0.329±0.002 |
| PTF | 0.184±0.003 | 0.185±0.004 | 0.144±0.005 | 0.138±0.007 | 0.044±0.003 | 0.047±0.002 | 0.287±0.004 | 0.292±0.007 |
| DATSING | 0.184±0.004 | 0.189±0.005 | 0.137±0.003 | 0.149±0.009 | 0.049±0.002 | 0.052±0.004 | 0.301±0.008 | 0.305±0.008 |
| RDA-DANN | 0.181±0.009 | 0.180±0.004 | 0.133±0.005 | 0.135±0.007 | 0.047±0.005 | 0.053±0.002 | 0.297±0.004 | 0.287±0.009 |
| RDA-ADDA | 0.174±0.005 | 0.181±0.003 | 0.134±0.002 | 0.142±0.003 | 0.045±0.003 | 0.049±0.003 | 0.281±0.001 | 0.287±0.002 |
| RDA-MMD | 0.186±0.004 | 0.179±0.004 | 0.140±0.006 | 0.144±0.003 | 0.045±0.003 | 0.052±0.004 | 0.291±0.004 | 0.289±0.003 |
| DAF | 0.169±0.002 | 0.176±0.004 | 0.125±0.008 | 0.123±0.005 | 0.042±0.004 | 0.049±0.003 | 0.277±0.005 | 0.280±0.007 |

Table 6: Performance comparison of DAF to all baselines on real-world benchmark datasets. The winners and the competitive followers (the gap is smaller than its standard deviation over 5 runs) are bolded for reference.

We also provide visualizations of forecasts for both synthetic and real-world experiments. Figure 9 provides more samples for the few-shot experiment where $N = 20$ as a complement to Figure 4. We see that DAF is able to approximately capture the sinusoidal signals even if the input is contaminated by white noise in most cases, while AttF fails in many cases. Figure 10 illustrates the performance gap between DAF and AttF in the experiment with source data *elec* and target data *traf* as an example in real scenarios. While AttF generally captures daily patterns, DAF performs significantly better.

| \mathcal{D}_T | \mathcal{D}_S | DAF | Cai et al. | Lead(%) |
|-----------------|-----------------|--------------|--------------|---------|
| <i>traf</i> | <i>elec</i> | 0.141 | 0.145 | 2.7 |
| | <i>wiki</i> | 0.161 | 0.154 | -4.5 |
| <i>elec</i> | <i>traf</i> | 0.056 | 0.061 | 8.2 |
| | <i>sales</i> | 0.084 | 0.089 | 5.2 |
| <i>wiki</i> | <i>sales</i> | 0.040 | 0.049 | 18.4 |
| | <i>traf</i> | 0.040 | 0.044 | 9.1 |
| <i>sales</i> | <i>wiki</i> | 0.251 | 0.237 | -5.9 |
| | <i>elec</i> | 0.268 | 0.284 | 5.6 |

Table 7: Comparison between Cai et al. [2021] and DAF on one-step ahead prediction tasks.

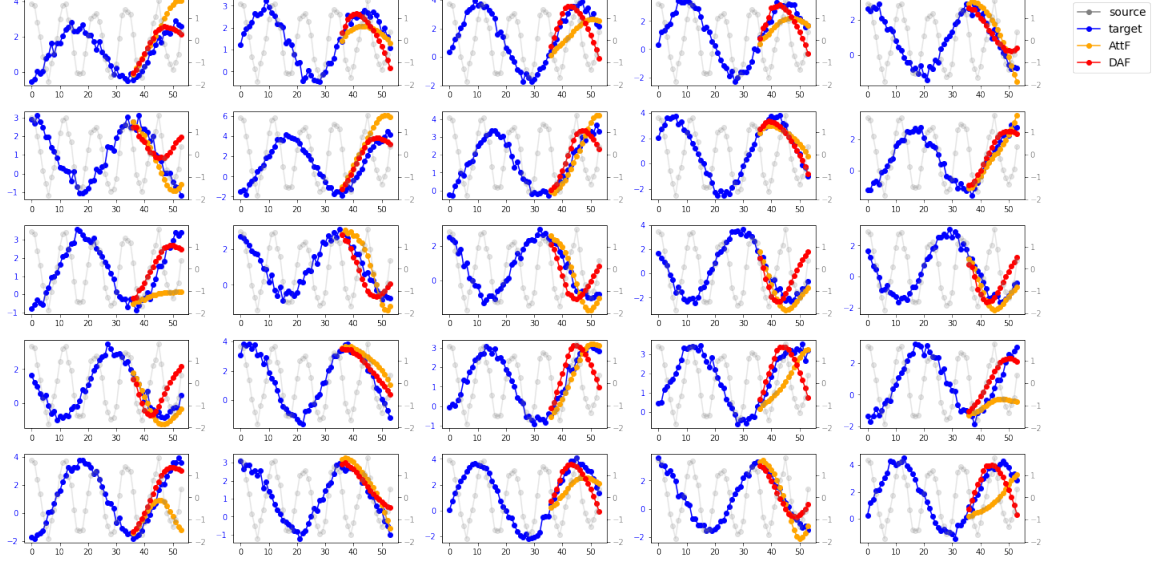


Figure 9: Test samples in the synthetic few-shot experiment where $N = 20$. The y-axis corresponding to the source is shown in grey, and that for the target in blue.

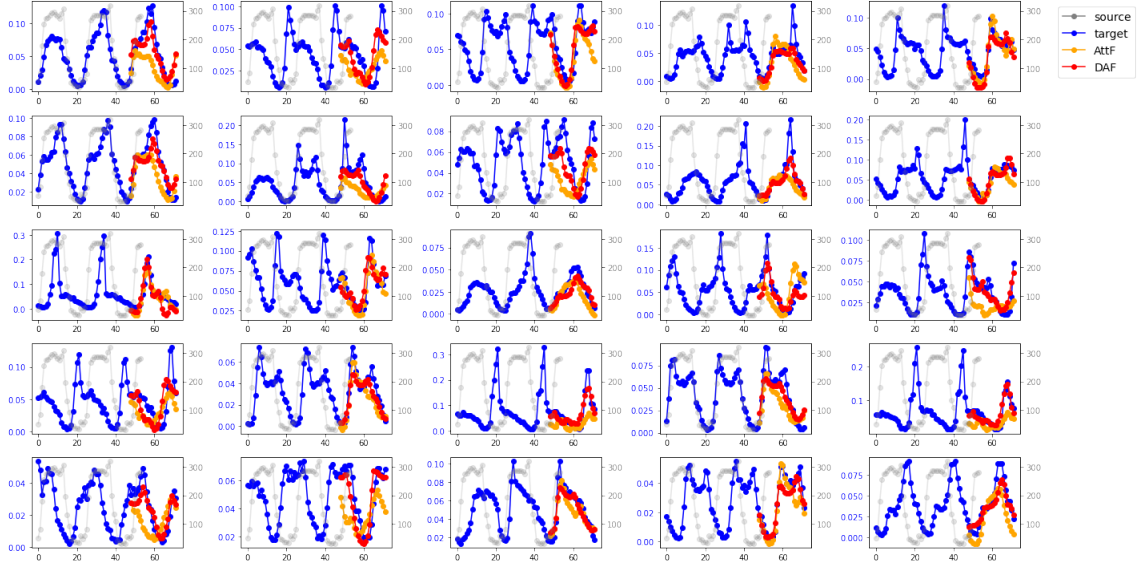


Figure 10: Test samples with source data *elec* and target data *traf* experiment. The y-axis corresponding to the source is shown in grey, and that for the target in blue.